



Effects of water adsorption on properties of electron-beam HfO₂/SiO₂ high-reflection coatings

Tingting Zeng^{a,b,c}, Meiping Zhu^{a,b,c,*}, Yingjie Chai^d, Chaoyi Yin^{a,b,c}, Nuo Xu^{a,b,c}, Kui Yi^{a,c}, Yanzhi Wang^{a,c}, Yuanan Zhao^{a,c}, Guohang Hu^{a,c}, Jianda Shao^{c,e,*}

^a Laboratory of Thin Film Optics, Shanghai Institute of Optics and Fine Mechanics, Chinese Academy of Sciences, Shanghai 201800, China

^b Center of Materials Science and Optoelectronics Engineering, University of Chinese Academy of Sciences, Beijing 100049, China

^c Key Laboratory of Materials for High Power Laser, Shanghai Institute of Optics and Fine Mechanics, Chinese Academy of Sciences, Shanghai 201800, China

^d CREOL, The College of Optics and Photonics, University of Central Florida, Orlando, FL 32816, USA

^e CAS Center for Excellence in Ultra-intense Laser Science, Shanghai 201800, China

ARTICLE INFO

Keywords:

Electron-beam coating
Water adsorption
Water vapor transmission rate
Fourier transform infrared spectroscopy
Stress
Aging behavior

ABSTRACT

The moisture-induced instability of electron-beam (e-beam) coating can even result in the performance instability of a large laser system. A dense plasma-ion-assisted-deposition SiO₂ capping layer was employed to isolate the top surface of the coating from ambient humidity and extend the originally rapid water adsorption process, allowing a deeper understanding of the instability of e-beam coatings caused by moisture. Spectral measurements suggested that four water adsorption steps, including filling, stabilization, swelling and refilling, led to the overall redshift and short-term fluctuations in spectra. The stress and Fourier transform infrared analysis revealed that water adsorption and ice-like/ice structure water was responsible for the increasing compressive stress evolution at the first stage and subsequent transition from compressive to tensile stress evolution, respectively. A model based on the finite element method was proposed to calculate the water vapor transmission rate of e-beam coatings. Our study on the underlying mechanism of moisture-induced instability of e-beam coating is helpful to ensure the reliability and stability of large laser systems.

1. Introduction

Large laser facilities, such as National Ignition Facility [1], Laser Megajoule [2] and Laser Interferometers Gravitational Observatory [3], are at the heart of energy programs towards sustainable energy and high precision detection. Electron-beam (e-beam) deposited large-aperture high-reflection multilayer coatings are key components in those large laser facilities, steering the laser from the amplifiers to the final optical assembly [4,5]. Due to the porous nature, the properties of the e-beam coating are sensitive to ambient humidity [6–9]. The aging effect occurs when the porous coatings are stored in an atmosphere environment [10]. The variation of environmental relative humidity will cause changes in spectrum and stress [11,12]. Spectral shift may vary the electric-field intensity distribution and therefore reduce the laser-resistance of the coating [13,14]. Change in stress may induce wave-front distortions [11,15,16] and affect beam quality of the system.

Issues respect to environmental instability of e-beam coating are

inevitable and may even degrade the performance and stability of the entire laser system. Much work has been done to qualitatively/quantitatively study the effect of variations in ambient humidity on the spectrum and stress, as well as moisture-related stress aging behaviors [11,14,17–19]. The adsorption and/or desorption of water molecules is the main cause of e-beam coating performance instability [20]. When transferred from vacuum to the atmospheric environment, the coating stress induced by water adsorption, either compressive or tensile, largely depends on the coating composition and deposition conditions [21]. A hydration mechanism between adsorbates and coating materials, categorized as irreversible chemical adsorption, was proposed to interpret the logarithmic kinetics of stress evolution during ambient air exposure [22]. Dense amorphous diffusion barriers, such as Al₂O₃ layers, were incorporated in traditional e-beam coating to reduce unwanted water-induced effects [15]. However, the water adsorption during coating exposure from the vacuum chamber to the air environment is almost “instantaneous” [20,23]. The ex-situ investigated coatings have absorbed a large amount of moisture before being taken

* Corresponding authors at: Laboratory of Thin Film Optics, Shanghai Institute of Optics and Fine Mechanics, Chinese Academy of Sciences, Shanghai 201800, China.

E-mail addresses: bree@siom.ac.cn (M. Zhu), jdshao@siom.ac.cn (J. Shao).

<https://doi.org/10.1016/j.tsf.2020.137826>

Received 30 August 2019; Received in revised form 10 December 2019; Accepted 26 January 2020

Available online 27 January 2020

0040-6090/© 2020 Elsevier B.V. All rights reserved.

out of the coating chamber; even for the in-situ stress investigation, the water adsorption happened too fast during the chamber venting process [17,23], which makes the moisture-sensitive properties related to the water vapor transmission rate (WVTR) and the underlying mechanism not easy to get.

Currently available WVTR measurement approaches, which are limited to tritiated water (T_2O) based radioactive element tracking, humidity sensor instruments, and calcium pad corrosion tests [24–27], might not be suitable for e-beam coatings. Humidity sensor instruments require coatings on flexible and permeable substrates, which is quite different from the impermeable glass-substrate coatings for the laser system. The calcium pad corrosion test allows glass-substrate coatings, but the test device demands strictly on sample preparation environment which is incompatible with the e-beam coating process.

In this work, a dense plasma-ion-assisted-deposition (PIAD) SiO_2 capping layer was proposed to reduce the water-accessible surface of e-beam coating by isolating the top surface from ambient humidity. The capped top surface extended the originally rapid water adsorption process of e-beam coating because water can only penetrate the side-walls of the coating, which made it possible to measure or trace the WVTR of e-beam coating. At the same time, a deeper understanding of the moisture-induced instability of e-beam coating was achieved. A detailed study of water molecule content and structure evolution based on Fourier transform infrared (FTIR) analysis and the corresponding effects on the spectral and mechanical properties of the coating were presented. A WVTR calculation model applicable to e-beam coatings was proposed.

2. Experimental details

2.1. Sample preparation

Six sets of coatings were deposited on BaF_2 (ϕ 30 mm \times 1.5 mm), BK7 (ϕ 30 mm \times 3 mm) and ZF7 (ϕ 30 mm \times 3 mm) substrates using a Leybold e-beam coater for FTIR, stress and spectral measurements, respectively. HfO_2 and SiO_2 , widely used in high-power laser and complementary metal oxide semiconductor applications [28–31], were used as high and low refractive index coating materials, which were deposited from metal Hf and SiO_2 , respectively. The design structures of the coatings are listed in Table 1. “G” and “A” represent substrate and air, respectively. “H”, “L” and “C” represent HfO_2 , SiO_2 and Capping SiO_2 with a quarter-wave optical thickness at a reference wavelength of 1064 nm. The physical thicknesses are $d_{4L} = 739$ nm, $d_{4C} = 705$ nm, $d_{3.35H} = 500$ nm, $d_{1.65C} = 291$ nm, $d_{5.42L} = 1000$ nm, $d_H = 149$ nm and $d_L = 185$ nm.

H and L layers were deposited using e-beam evaporation, while C layer was deposited using PIAD at a bias voltage of 170 V. Prior to deposition, the vacuum chamber was evacuated to a base pressure of 9×10^{-4} Pa and heated to 200 °C. The deposition rates of H, L and C layers were 0.14 nm/s, 0.6 nm/s and 0.4 nm/s, respectively. The oxygen pressures of H and L layers were 1.4×10^{-2} Pa and 5.5×10^{-3} Pa, respectively. An Ar/O_2 mixture with pressure of about 3×10^{-2} Pa was used for C layer.

Table 1
Design structure and substrate information for the coatings.

Sample	Coating design	Substrate (refractive index at 1064 nm)
S1	G/4 L/A	ZF7 (1.78)
S2	G/4C/A	ZF7/BK7 (1.78/1.51)
B1	G/3.35H1.65C/A	BaF_2 /BK7 (1.47/1.51)
B2	G/5.42L1.65C/A	BaF_2 /BK7/ZF7 (1.47/1.51/1.78)
M1	G/4L(HL) 12 H4L/A	BK7 (1.51)
M2	G/4L(HL) 12 H4C/A	BK7 (1.51)

2.2. Sample characterization

All samples were stored and characterized in a Class 1000 clean room with a controlled temperature of 23 ± 1.5 °C and a relative humidity of $45 \pm 5\%$. Atomic force microscopy (AFM; Veeco Dimension 3100) was used to characterize the surface morphologies of prepared samples, and the surface pore size distributions were analyzed by a functional module in AFM image analysis software. A Perkin-Elmer Lambda 1050 spectrometer was used to measure the transmission spectra. Commercial thin film software Optilayer was employed to extract the refractive indices of HfO_2 and SiO_2 layers. The evolution of hydroxyl groups (-OH) related vibration mode was investigated by a Fourier transform infrared spectrometer (FTIR; Bruker, VERTEX 70). The residual stress evolutions of samples were inspected by an optical interferometer (ZYGO Mark III-GPI).

3. Results and discussions

3.1. Surface morphologies and pore distributions

The surface morphologies of prepared samples were investigated by AFM at tapping mode. An area of $5 \mu m \times 5 \mu m$ was sampled. As shown in Fig. 1, the surface morphologies of coatings with capping layer exhibited much smaller pore sizes than those without capping layer. The surface pore distribution statistics of coatings with capping layer followed a narrower distribution which located mainly in the range of < 50 nm. Conventional e-beam coatings tend to exhibit porous microstructure while PIAD techniques can significantly improve the compactness of the coating, reducing the number or size of pores in coating via energetic ion bombardment [32]. This result implied that the PIAD SiO_2 capping layer possessed a good waterproof property owing to relatively high compactness.

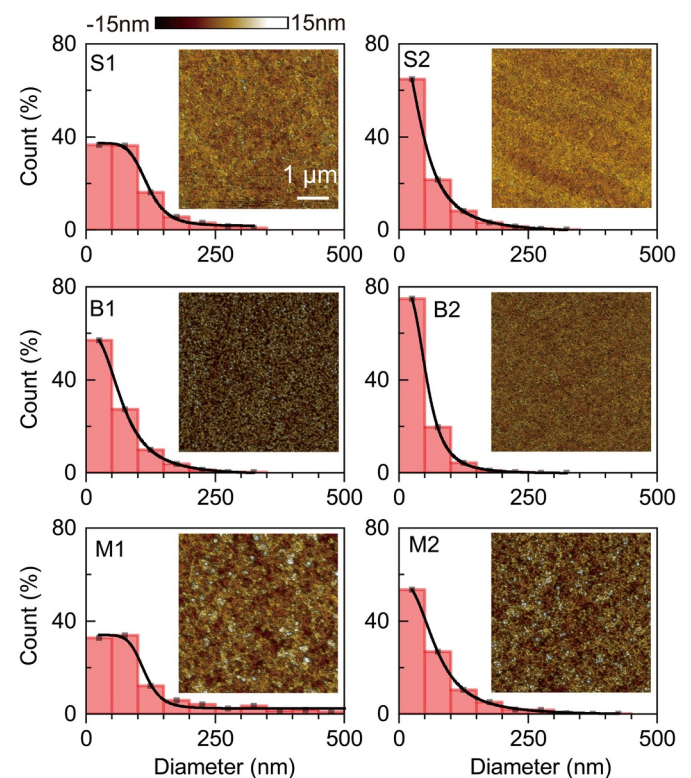


Fig. 1. Surface morphologies and pore distribution statistics of prepared samples, the fitted black curves followed a logistic distribution.

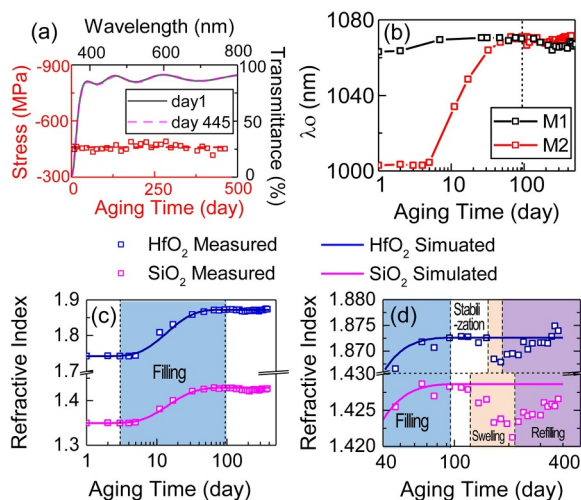


Fig. 2. (a) Stress and spectra aging behavior of S2. (b) Wavelengths at peak reflectivity of M1 and M2 versus aging time. (c) Refractive indices (at 1064 nm) of HfO₂ and SiO₂ layers in M2 versus aging time. (d) Magnification of the certain area in (c), the background color blocks indicated the four successive steps.

3.2. Spectral shifts and refractive indices evolution

Transmission spectra were measured at normal incident regularly to monitor the spectral shift. Both the optical and stress aging behavior of the capping layer, indicated its good long-term stability, as shown in Fig. 2(a). The capping layer could be a good water molecule barrier on the surface of e-beam coating. In this case, water molecules can only penetrate through the sidewall of coating. Geometrically, the sidewall area was about three or four orders of magnitude (depending on the physical thickness of coating) smaller than that of the top surface, which significantly extended the water adsorption saturation time. Coating M2, the multilayer coating with a capping layer, took about 90 days, while coating M1, the multilayer coating without a capping layer, took just a few days to be spectral stable, as shown in Fig. 2(b).

Refractive indices of HfO₂ and SiO₂ layers in sample M2 at 1064 nm were extracted by commercial thin-film software Optilayer, and an absorbing inhomogeneous model was applied [33]. The refractive indices versus aging time were depicted in Fig. 2(c and d), revealing that the water transport process could be divided into four successive steps, namely filling, stabilization, swelling and refilling [34,35]. As-deposited e-beam coatings owned lowest refractive indices because they were water-free and consist of only coating matrix and unoccupied pores. The refractive indices increased with increasing incorporation of water molecules into the inter initially vacuum pores until the water transport reached a relative equilibrium state. Then the refractive indices fell back slightly as a large amount of accumulated permeant water widening the free volume of coating matrix, which in turn provided new space for the water molecule filling. In our case, the swelling and refilling in SiO₂ layers were much obvious than in HfO₂ layers, which indicated that the coating matrix strength of the HfO₂ layer was higher than the SiO₂ layer. It took about four days for water molecules to penetrate from the periphery to the measured central region of capped e-beam coating, which accounts for the flat part of the curves shown in Fig. 2(b and c). The different water transport steps would lead to different coating stress behavior and will be discussed later in Section 3.4.

3.3. FTIR analysis

FTIR analysis was conducted on sample B1 and B2 to investigate the structural evolution of absorbed water molecules, as well as their

Table 2
Hydroxyl groups of different structure.

Peak	Vibration mode	Wavenumber (cm ⁻¹)
I	-OH in isolated Si-OH	3660 [37]
II	-OH in Si-OH hydrogen bonded with neighboring -OH	3547 [38]
III	-OH in a water molecule (free H ₂ O included) with a low number of hydrogen bonds	3428 [39]
IV	-OH stretch of regular liquid H ₂ O structure	3281 [39]
V	-OH stretch of ice-like structure	3230 [40]
IV	-OH collective mode of ice lattice	3150 [40]

impact on micro properties of HfO₂ and SiO₂ layers. IR transmittance spectra were recorded from 4000 cm⁻¹ to 400 cm⁻¹ at a resolution of 4 cm⁻¹, and the absorbance was derived using Beer-Lambert Law [36]:

$$A = -\log \frac{I}{I_0} = \epsilon lc \quad (1)$$

where, A is absorbance of the FTIR spectra, I_0 and I represent the incident and transmitted light intensities, ϵ denotes the molar absorptivity of tested material, l is the light path distance, and c is molar concentration. Since the thicknesses of the tested samples in our case were fixed, higher absorption peak intensity indicated a higher target component was formed as the exposure time increases.

According to Table 2, the typical water-related infrared absorption peaks, -OH in our case, lies in the range of 2700–3800 cm⁻¹. The -OH vibration modes increased in peak intensity and peak number over time. As compared in Fig. 3, in both HfO₂ and SiO₂ layers, the intensity of the overall water-related absorption band increased with increasing water infiltration, and the peak absorbance shifted to the lower wavenumber as the degree of hydrogen bonding increases. The faster increase and shift of the overall peak absorbance in HfO₂ layers can be explained by that HfO₂ layers are less dense compared to SiO₂ layers, contributing to higher WVTR.

For one coating material, not only the content but also the structure of the absorbed water increased with aging time. Take the bilayer coating B2 for example, the IR spectra band at different aging times were deconvoluted into the peaks listed in Table 2 and were shown in Fig. 4. Peaks I–IV were observed on day 13, peaks I–V were observed on day 54, and peaks I–VI were observed on day 132.

The increases in peak intensity and peak number revealed that the structure of absorbed water molecules transitioned from being bound by silicon on pore walls, through the liquid phase and towards ice-like or ice structure as time goes. Water molecules in the bilayer sample B1 showed a similar but relatively fast evolution process due to relatively fast water transport in the HfO₂ layer. The observed phenomenon can be explained as follows: H₂O is Lewis base while the Si atoms and Hf atoms on the coating pore walls act as Lewis acid center, providing

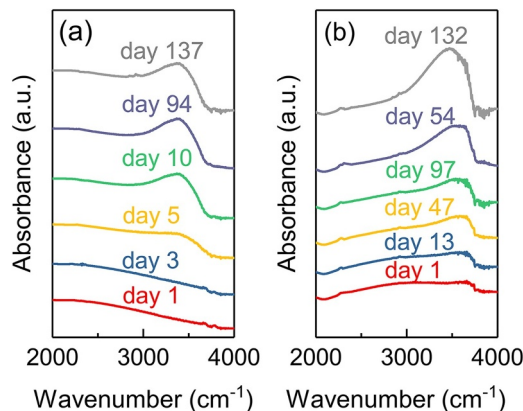


Fig. 3. FTIR analysis of bilayers: -OH absorption regions in (a) B1 and (b) B2.

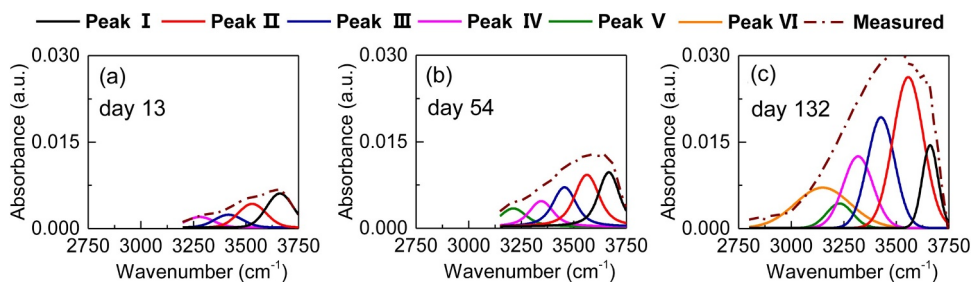


Fig. 4. Deconvolution of absorption spectra in B2 at different aging time.

active sites to form Si-OH or Hf-OH with adsorbed H₂O molecule. Meanwhile, the dissociated proton reacts with the adjacent oxygen, which contributes to the formation of Si-OH or Hf-OH too. As the number of water molecules entering the capped coating increases, hydrogen bonds begin to form both between water molecule-water molecule and Si/Hf-OH-water molecule. As time goes by, the degree of hydrogen bonding increases with the increasing water infiltration, which accounts for the configuration evolution of adsorbed water molecules.

Porous coatings consist of matrix and pores. Changes in the coating matrix can be reflected by the ratio of Si-O-Si performing 180° out-of-phase (AS₂) to in-phase (AS₁) asymmetric stretching, as illustrated in Fig. 5(a), and the relatively large ring size of the coating matrix network structure contributes to AS₂ mode [41,42]. The higher the AS₂-to-AS₁ ratio, the less structural order and coating densification [35,43]. The AS₂/AS₁ in bilayer coating B2 increased with aging time, as presented in Fig. 5(b), indicating that the SiO₂ component with a relatively large ring sizes took an increasing proportion in the coating matrix. In our case, the relaxation in the SiO₂ matrix was enhanced.

3.4. Stress aging behavior

Surface figures were determined by an optical interferometer, and coating stress was extracted by Stoney's equation [20]:

$$\sigma = \frac{E_s t_s^2}{6(1 - \nu_s) t_f} \left(\frac{1}{R_2 - R_1} \right) \quad (2)$$

where, E_s and ν_s are Young's modulus and Poisson's ratio of the substrate; t_s and t_f stand for the thickness of substrate and coating on it; R_1 and R_2 represent the radius of substrate curvature before and after deposition.

As shown in Fig. 6, compared to the compressive initial residual stress of the bilayer coating B2, the initial residual stress of the bilayer coating B1 was tensile, but they both evolved in the direction of compressive stress first. The stress behavior of multilayer sample M2 can be considered as a combination of the coating B1 and B2. The residual stress of the coating M2 with capping layer initially evolved compressively, while the compressive residual stress of the conventional coating M1 without capping layer continuously released over time. The content and structures of adsorbed water molecules induced aging in coating stress both physically and chemically. At the beginning of air exposure, adsorption of moisture reduced the surface energy, and the water

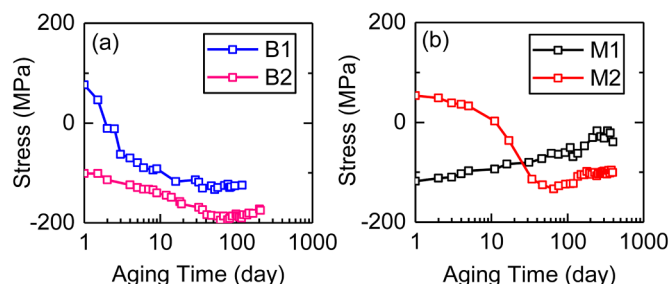


Fig. 6. Residual stress evolution as a function of the logarithm of aging time for (a) B1, B2 and (b) M1, M2.

molecules tended to generate repulsion of the permanent electric dipole moments, which physically introduced the compressive stress of the multilayer coatings [6,11,18].

After the day ~60, the stress evolution of the coating M2 with capping layer turned into tensile dominant. The tensile component was introduced due to the following reasons:

- (1) Chemically, hydration reaction intensified because of the daily concentrated water molecules.
- (2) Swelling-induced coating matrix relaxation intensified because a large amount of permeant water widened the free volume of the coating matrix.
- (3) The ice-like/ice structure of H₂O has a lower density than the liquid phase (8.3% less).

4. WVTR calculation model

A schematic diagram of water transport in coatings with a capping layer is shown in Fig. 7(a). The domain colored in pink was accessible for diffusion of water molecular. A model based on effective medium approximation method [44] was proposed to extract the value of WVTR. The underlying assumption is that e-beam coatings consist of material matrix and water-accessible pores.

Pores were initially unoccupied and finally filled with water molecules after long-term air exposure. Here, we used f as the total pore volume fraction; $p(R = 0, t)$ ($0 \leq p(R = 0, t) \leq f$) as the time-dependent volume fraction of pores occupied by water molecules at the center of coating M2. The measured refractive index $n(R = 0, t)$ should follow:

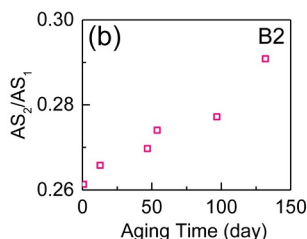
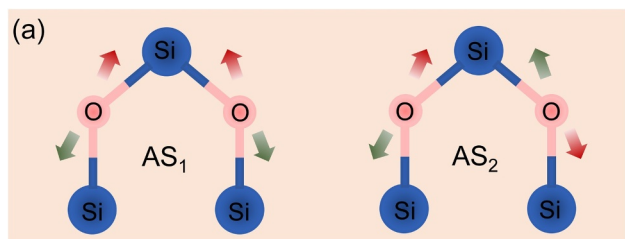


Fig. 5. (a) Schematic diagram of Si-O-Si asymmetric stretching mode, in which adjacent oxygen atoms are performing in-phase (AS₁) and 180° out-of-phase (AS₂) asymmetric stretching. The colored arrows beside the oxygen atoms express the stretching direction of the oxygen atom. (b) Evolution of AS₂/AS₁ in B2.

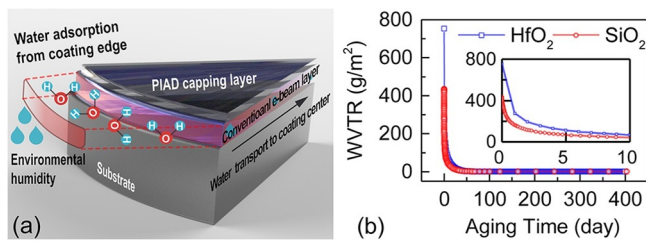


Fig. 7. (a) Schematic diagram of water transport in coating with a capping layer. (b) WVTR of HfO₂ and SiO₂ layers in M2 versus aging time. The inset shows the data for the first 20 days.

$$n(R = 0, t) = (1 - f)n_{\text{matrix}} + p(R = 0, t)n_{\text{water}} + [f - p(R = 0, t)]n_{\text{void}} \quad (3)$$

$$f = \frac{n_{\text{stable}} - n_{\text{initial}}}{n_{\text{water}} - n_{\text{void}}} \quad (4)$$

where, n_{matrix} , n_{water} and n_{void} are constants that represent refractive indices of the coating matrix, water and unoccupied pores, respectively. n_{initial} (when $t = 0$ and $p(R = 0, t) = 0$) and n_{stable} (when $t = \infty$ and $p(R = 0, t) = f$) are the refractive indices measured as-deposited and at steady state (ignoring the swelling and refilling steps), respectively. The measured refractive index profiles shown in Fig. 2(c) followed the shape of a Fickian diffusion [45,46], and can be used to simulate the adsorption process. Using $p(R = 0, t)$ calculated by Eq. (3), the localized rule of water transport can be given by second Fick's law of diffusion [47]:

$$\frac{\partial c(R, t)}{\partial t} + \nabla \cdot [-D \nabla c(R, t)] = 0 \quad (5)$$

$$c(R = 0, t) = \frac{\rho_{\text{water}}}{M_{\text{H}_2\text{O}}} p(R = 0, t) \quad (6)$$

$$p(R, t) = \begin{cases} 0 & t = 0 \& R < R_{\text{inlet}} \\ f & t = \infty \& R < R_{\text{inlet}} \\ f & t \geq 0 \& R = R_{\text{inlet}} \end{cases} \quad (7)$$

where, D is the diffusion coefficient of the water molecules. $c(R, t)$ denoted molar concentration of H₂O at the radius R at time t , and the concentration versus aging time at the central point of the coating M2 can be given by Eq. (6). $M_{\text{H}_2\text{O}}$ and ρ_{water} are constants that represent the molar mass of H₂O and the mass density of water, respectively. A water molecule inlet boundary condition was applied at the boundary ($R = R_{\text{inlet}}$) of the water-accessible domain, which is the sidewall of the capped coating. The most fitted water diffusion coefficients of SiO₂ and HfO₂ were $2.3(\pm 0.1) \times 10^{-11}$ m²/s and $2.40(\pm 0.1) \times 10^{-11}$ m²/s, respectively. As shown in Fig. 2(c), the simulated refractive index curves agreed with the discrete measured data. The water diffusion coefficient in silica glass of the order of 10^{-25} m²/s has been reported [48,49] while little attention has been paid to the water diffusion coefficient in the coating form of SiO₂ and HfO₂. Tsui et al. reported the water diffusion coefficient in organosilicate glass film stacks as 1.4×10^{-11} m²/s [50], which shared the same order of magnitudes with the inorganic dielectric film in this work.

With the water diffusion coefficient D , the WVTR can be calculated by:

$$WVTR(R = R_{\text{inlet}}, t) = -\vec{n} \cdot [-D \nabla c(R = R_{\text{inlet}}, t)] M_{\text{H}_2\text{O}} \quad (8)$$

where, \vec{n} represents the surface unit normal vector pointing out. Here we got the transient variation of $WVTR(R = R_{\text{inlet}}, t)$ at the coating boundary over time, as presented in Fig. 7(b). The concentration gradient of water molecules inside and outside the capped coating decreased over time, which resulted in the reduction in WVTR. The general WVTR (intersection of the WVTR curve and Y-axis) of e-beam HfO₂ and SiO₂ layers in this work were about 754 and 434 g/m²/day, respectively.

5. Conclusion

In conclusion, a dense capping layer prepared using PIAD was proposed to isolate the top surface of a conventional e-beam coating from ambient moisture. The proposed dense PIAD capping layer extended the originally rapid water adsorption process, allowing a deeper understanding of the instability of e-beam coatings caused by moisture. The experimental results suggested that the water transport in e-beam coatings could be divided into four successive steps: filling, stabilization, swelling and refilling. The water molecule content and structure evolution led to the overall redshift and short-term fluctuations in spectra, as well as the increasing compressive stress evolution at the first stage and subsequent transition from compressive to tensile stress evolution. A WVTR model suitable for most porous coatings was proposed to calculate the WVTR of the e-beam coating. In this work, the WVTR of HfO₂ and SiO₂ layers was about 754 and 434 g/m²/day, respectively. Capping both the top and sidewall of the e-beam coating with a dense layer might be a promising way to obtain a e-beam coating with better stability, and therefore improve the stability of laser system.

CRediT authorship contribution statement

Tingting Zeng: Methodology, Validation, Formal analysis, Investigation, Data curation, Visualization, Writing - original draft, Writing - review & editing. **Meiping Zhu:** Conceptualization, Methodology, Formal analysis, Resources, Writing - review & editing, Supervision, Project administration, Funding acquisition. **Yingjie Chai:** Writing - original draft, Formal analysis. **Chaoyi Yin:** Formal analysis. **Nuo Xu:** Formal analysis. **Kui Yi:** Resources, Supervision. **Yanzhi Wang:** Resources. **Yuanan Zhao:** Resources. **Guohang Hu:** Resources. **Jianda Shao:** Resources, Supervision, Funding acquisition.

Declaration of Competing Interest

The authors declare that they have no known competing financial interests or personal relationships that could have appeared to influence the work reported in this paper.

Acknowledgements

This work was supported by National Special Support Program for Young Top-notch Talent; National Natural Science Foundation of China (61975215); Youth Innovation Promotion Association of the Chinese Academy of Sciences; Shanghai Young Top-notch Talent Program; Strategic Priority Research Program of the Chinese Academy of Sciences (XDB16030400).

References

- [1] R.A. Zacharias, N.R. Beer, E.S. Bliss, S.C. Burkhart, S.J. Cohen, S.B. Sutton, R.L. Van Atta, S.E. Winters, J.T. Salmon, M.R. Latta, Alignment and wavefront control systems of the National Ignition Facility, *Opt. Eng.* 43 (2004) 2873–2885, <https://doi.org/10.1117/1.1815331>.
- [2] D. Besnard, The megajoule laser program – ignition at hand, *Eur. Phys. J. D* 44 (2007) 207–213, <https://doi.org/10.1140/epjd/e2006-00165-4>.
- [3] B.P. Abbott, R. Abbott, T.D. Abbott, et al., (with another 1045 authors listed at the original Letter) LIGO Scientific and Virgo Collaboration, GW170104: observation of a 50-Solar-Mass binary black hole coalescence at redshift 0.2, *Phys. Rev. Lett.* 118 (2017) 221101, <https://doi.org/10.1103/PhysRevLett.118.221101>.
- [4] J.H. Campbell, R.A. Hawley-Fedder, C.J. Stolz, J.A. Menapace, M.R. Borden, P.K. Whitman, J. Yu, M.J. Runkel, M.O. Riley, M.D. Feit, R.P. Hackel, NIF optical materials and fabrication technologies: an overview, in: M.A. Lane, C.R. Wuest (Eds.), *Optical Engineering at the Lawrence Livermore Nation Laboratory II: The National Ignition Facility*, 2004, <https://doi.org/10.1117/12.538471> San Jose, CA, United States May 28 International Society for Optics and Photonics, Proc. SPIE 5341 (2004) 84–101.
- [5] C.J. Stolz, M.J. Runkel, M.S. McBurney, R.E. Cheek, J.A. Menapace, Metrology of mirrors for the National Ignition Facility, in: M.A. Lane, C.R. Wuest (Eds.), *Optical Engineering at the Lawrence Livermore Nation Laboratory II: The National Ignition Facility*, 2004, <https://doi.org/10.1117/12.538472> San Jose, CA, United States May 28 International Society for Optics and Photonics, Proc. SPIE 5341 (2004) 114–120.

- [6] H.A. Macleod, Microstructure of optical thin films, in: R.I. Seddon (Ed.), *Optical Thin Films*, 1982, <https://doi.org/10.1117/12.933282> Los Angeles, United States April 29 International Society for Optics and Photonics, Proc. SPIE 0325 (1982) 21–28.
- [7] M. Yang, W. Xie, Y. Dai, D. Lee, J. Dai, Y. Zhang, Z. Zhuang, Dielectric multilayer-based fiber optic sensor enabling simultaneous measurement of humidity and temperature, *Opt. Express* 22 (2014) 11892–11899, <https://doi.org/10.1364/oe.22.011892>.
- [8] D.E. Morton, T.R. Jensen, Ion-assisted deposition of moisture stable HfO₂ thin-films, *Opt. Interf. Coat. Opt. Soc. Am.* (2001) 40–42.
- [9] O. Stenzel, S. Wilbrandt, N. Kaiser, M. Vinnichenko, F. Munnik, A. Kolitsch, A. Chuvilin, U. Kaiser, J. Ebert, S. Jakobs, A. Kaless, S. Wüthrich, O. Treichel, B. Wunderlich, M. Bitzer, M. Grössl, The correlation between mechanical stress, thermal shift and refractive index in HfO₂, Nb₂O₅, Ta₂O₅ and SiO₂ layers and its relation to the layer porosity, *Thin Solid Films* 517 (2009) 6058–6068, <https://doi.org/10.1016/j.tsf.2009.05.009>.
- [10] M.G. Beghi, C.E. Bottani, L. Calliari, M. Bonelli, A. Miotello, P.M. Ossi, J. Kovac, G. Scarel, M. Sancrotti, Ageing effects of thin films prepared by ion beam assisted deposition: a multi-technique characterization, *Thin Solid Films* 290 (1996) 401–405, [https://doi.org/10.1016/S0040-6090\(96\)09133-X](https://doi.org/10.1016/S0040-6090(96)09133-X).
- [11] C.J. Stolz, J.R. Taylor, W.K. Eickelberg, J.D. Lindh, Effects of vacuum exposure on stress and spectral shift of high reflective coatings, *Appl. Opt.* 32 (1993) 5666–5672, <https://doi.org/10.1364/ao.32.005666>.
- [12] M. Zhu, K. Yi, D. Arhlinger, H. Qi, J. Shao, Effect of Advanced Plasma Source bias voltage on properties of HfO₂ films prepared by plasma ion assisted electron evaporation from metal hafnium, *Thin Solid Films* 540 (2013) 17–22, <https://doi.org/10.1016/j.tsf.2013.05.118>.
- [13] W.H. Lowdermilk, D. Milam, F. Rainer, Optical coatings for laser fusion applications, *Thin Solid Films* 73 (1980) 155–166, [https://doi.org/10.1016/0040-6090\(80\)90342-9](https://doi.org/10.1016/0040-6090(80)90342-9).
- [14] W. Riede, P. Allenspacher, L. Jensen, M. Jupé, Analysis of the air-vacuum effect in dielectric coatings, in: G.J. Exarhos, D. Ristau, M.J. Soileau, C.J. Stolz (Eds.), *Laser-Induced Damage in Optical Materials*, 2008, <https://doi.org/10.1117/12.804095> Boulder, Colorado, United States December 30, International Society for Optics and Photonics, Proc. SPIE 7132 (2008) 71320F.
- [15] J.B. Oliver, P. Kupinski, A.L. Rigatti, A.W. Schmid, J.C. Lambropoulos, S. Papernov, A. Kozlov, C. Smith, R.D. Hand, Stress compensation in hafnia/silica optical coatings by inclusion of alumina layers, *Opt. Express* 20 (2012) 16596–16610, <https://doi.org/10.1364/oe.20.016596>.
- [16] H. Liu, L. Jensen, P. Ma, D. Ristau, Stress compensated anti-reflection coating for high power laser deposited with IBS SiO₂ and ALD Al₂O₃, *Appl. Surf. Sci.* 476 (2019) 521–527, <https://doi.org/10.1016/j.apsusc.2019.01.125>.
- [17] E.H. Hirsch, Stress in porous thin films through adsorption of polar molecules, *J. Phys. D Appl. Phys.* 13 (1980) 2081–2094, <https://doi.org/10.1088/0022-3727/13/11/018>.
- [18] J.F. Anzellotti, D.J. Smith, R.J. Sczupak, Z.R. Chrzan, Stress and environmental shift characteristics of HfO₂/SiO₂ multilayer coatings, in: H.E. Bennett, A.H. Guenther, M.R. Kozlowski, B.E. Newnam, M.J. Soileau (Eds.), *Laser-induced Damage in Optical Materials*, 1997, <https://doi.org/10.1117/12.274221> Boulder, Colorado, United States May 13 International Society for Optics and Photonics, Proc. SPIE 2966 (1996) 258–264.
- [19] J.B. Oliver, J. Howe, A. Rigatti, D.J. Smith, C. Stolz, High precision coating technology for large aperture NIF optics, *Optical Interference Coatings*, Technical Digest Series, Optical Society of America, 2001, <https://doi.org/10.1364/OIC.2001.ThD2.ThD2>.
- [20] H. Leplan, B. Geenen, J.Y. Robic, Y. Pauleau, Residual stresses in evaporated silicon dioxide thin films: correlation with deposition parameters and aging behavior, *J. Appl. Phys.* 78 (1995) 962–968, <https://doi.org/10.1063/1.360290>.
- [21] H. Sankur, W. Gunning, Sorbed water and intrinsic stress in composite TiO₂-SiO₂ films, *J. Appl. Phys.* 66 (1989) 807–812, <https://doi.org/10.1063/1.343501>.
- [22] H. Leplan, J.Y. Robic, Y. Pauleau, Kinetics of residual stress evolution in evaporated silicon dioxide films exposed to room air, *J. Appl. Phys.* 79 (1996) 6926–6931, <https://doi.org/10.1063/1.361517>.
- [23] M. Fang, D. Hu, J. Shao, Evolution of stress in evaporated silicon dioxide thin films, *Chin. Opt. Lett.* 8 (2010) 119–122, <https://doi.org/10.3788/col20100801.0119>.
- [24] A.R. Coulter, R.A. Deeken, G.M. Zentner, Water permeability in poly(ortho ester)s, *J. Memb. Sci.* 65 (1992) 269–275, [https://doi.org/10.1016/0376-7388\(92\)87028-V](https://doi.org/10.1016/0376-7388(92)87028-V).
- [25] M.D. Kempe, Modeling of rates of moisture ingress into photovoltaic modules, *Sol. Energy Mater. Sol. Cells* 90 (2006) 2720–2738, <https://doi.org/10.1016/j.solmat.2006.04.002>.
- [26] P.F. Garcia, R.S. McLean, M.H. Reilly, M.D. Groner, S.M. George, Ca test of Al₂O₃ gas diffusion barriers grown by atomic layer deposition on polymers, *Appl. Phys. Lett.* 89 (2006) 1–4, <https://doi.org/10.1063/1.221912>.
- [27] Y.Q. Yang, Y. Duan, P. Chen, F.B. Sun, Y.H. Duan, X. Wang, D. Yang, Realization of thin film encapsulation by atomic layer deposition of Al₂O₃ at low temperature, *J. Phys. Chem. C* 117 (2013) 20308–20312, <https://doi.org/10.1021/jp406738h>.
- [28] G. He, X. Chen, Z. Sun, Interface engineering and chemistry of HF-based high-k dielectrics on III–V substrates, *Surf. Sci. Rep.* 68 (2013) 68–107, <https://doi.org/10.1016/j.surfrep.2013.01.002>.
- [29] J.W. Zhang, G. He, L. Zhou, H.S. Chen, X.S. Chen, X.F. Chen, B. Deng, J.G. Lv, Z.Q. Sun, Microstructure optimization and optical and interfacial properties modulation of sputtering-derived HfO₂ thin films by TiO₂ incorporation, *J. Alloy. Compd.* 611 (2014) 253–259, <https://doi.org/10.1016/j.jallcom.2014.05.074>.
- [30] G. He, J. Gao, H. Chen, J. Cui, Z. Sun, X. Chen, Modulating the interface quality and electrical properties of HfTiO/InGaAs gate stack by atomic-layer-deposition-derived Al₂O₃ passivation layer, *ACS Appl. Mater. Interfaces* 6 (2014) 22013–22025, <https://doi.org/10.1021/am506351u>.
- [31] G. He, J. Liu, H. Chen, Y. Liu, Z. Sun, X. Chen, M. Liu, L. Zhang, Interface control and modification of band alignment and electrical properties of HfTiO/GaAs gate stacks by nitrogen incorporation, *J. Mater. Chem. C* 2 (2014) 5299–5308, <https://doi.org/10.1039/C4TC00572D>.
- [32] R. Thielsch, A. Gatto, J. Heber, N. Kaiser, A comparative study of the UV optical and structural properties of SiO₂, Al₂O₃, and HfO₂ single layers deposited by reactive evaporation, ion-assisted deposition and plasma ion-assisted deposition, *Thin Solid Films* 410 (2002) 86–93, [https://doi.org/10.1016/S0040-6090\(02\)00208-0](https://doi.org/10.1016/S0040-6090(02)00208-0).
- [33] A.V. Tikhonravov, M.K. Trubetskov, T.V. Amotchkina, G. DeBell, V. Pervak, A.K. Sytchkova, M.L. Grilli, D. Ristau, Optical parameters of oxide films typically used in optical coating production, *Appl. Opt.* 50 (2011) C75–C85, <https://doi.org/10.1364/ao.50.000c75>.
- [34] W. Ogieglo, H. Wormeester, K.J. Eichhorn, M. Wessling, N.E. Benes, In situ ellipsometry studies on swelling of thin polymer films: a review, *Prog. Polym. Sci.* 42 (2015) 42–78, <https://doi.org/10.1016/j.progpolymsci.2014.09.004>.
- [35] A. Perrotta, Technische Universiteit Eindhoven, Ph.D. Thesis (2016).
- [36] C. Song, R. Huang, X. Wang, Y. Guo, J. Song, Tunable red light emission from a-Si:h/a-SiNx multilayers, *Opt. Mater. Express* 3 (2013) 664–670, <https://doi.org/10.1364/ome.3.000664>.
- [37] A. Brunet-Bruneau, J. Rivory, B. Rafin, J.Y. Robic, P. Chaton, Infrared ellipsometry study of evaporated SiO₂ films: matrix densification, porosity, water sorption, *J. Appl. Phys.* 82 (1997) 1330–1335, <https://doi.org/10.1063/1.365906>.
- [38] S. Rojas, L. Zanotti, A. Borghesi, A. Sassella, G.U. Pignatelli, Characterization of silicon dioxide and phosphosilicate glass deposited films, *J. Vac. Sci. Technol. B Microelectron. Nanomater. Struct.* 11 (1993) 2081–2089, <https://doi.org/10.1116/1.586546>.
- [39] T.Q. Luong, P.K. Verma, R.K. Mitra, M. Havenith, Onset of hydrogen bonded collective network of water in 1,4-dioxane, *J. Phys. Chem. A* 115 (2011) 14462–14469, <https://doi.org/10.1021/jp204927r>.
- [40] Y. Raichlin, A. Mollo, A. Katzir, Investigations of the structure of water using mid-IR fiberoptic evanescent wave spectroscopy, *Phys. Rev. Lett.* 93 (2004) 185703, <https://doi.org/10.1103/physrevlett.93.185703>.
- [41] C.T. Kirk, Quantitative analysis of the effect of disorder-induced mode coupling on infrared absorption in silica, *Phys. Rev. B* 38 (1988) 1255, <https://doi.org/10.1103/PhysRevB.38.1255>.
- [42] A. Lefevre, L.J. Lewis, L. Martinu, M.R. Wertheimer, Structural properties of silicon dioxide thin films densified by medium-energy particles, *Phys. Rev. B* 64 (2001) 225429, <https://doi.org/10.1103/PhysRevB.64.115429>.
- [43] C.Y. Wu, R.M. Liao, L.W. Lai, M.S. Jeng, D.S. Liu, Organosilicon/silicon oxide gas barrier structure encapsulated flexible plastic substrate by using plasma-enhanced chemical vapor deposition, *Surf. Coat. Technol.* 206 (2012) 4685–4691, <https://doi.org/10.1016/j.surfcoat.2012.05.080>.
- [44] K. Kinoshita, M. Nishibori, Porosity of MgF₂ films—evaluation based on changes in refractive index due to adsorption of vapors, *J. Vac. Sci. Technol.* 6 (1969) 730–733, <https://doi.org/10.1116/1.1315743>.
- [45] J.L.A. Mrotek, M.J. Matthewson, C.R. Kurkjian, Diffusion of moisture through fatigue and aging-resistant polymer coatings on lightguide fibers, *J. Lightw. Technol.* 21 (2003) 1775, <https://doi.org/10.1109/JLT.2003.814930>.
- [46] J.L.A. Mrotek, M.J. Matthewson, C.R. Kurkjian, Diffusion of moisture through optical fiber coatings, *J. Lightw. Technol.* 19 (2001) 988.
- [47] P.A. Johnson, A.L. Babb, Liquid diffusion of non-electrolytes, *Chem. Rev.* 56 (1956) 387–453.
- [48] F. Lechenault, C.L. Rountree, F. Cousin, J.P. Bouchaud, L. Ponson, E. Bouchaud, Evidence of deep water penetration in silica during stress corrosion fracture, *Phys. Rev. Lett.* 106 (2011) 165504, <https://doi.org/10.1103/PhysRevLett.106.165504>.
- [49] M. Tomozawa, K.M. Davis, Time dependent diffusion coefficient of water into silica glass at low temperatures, *Mater. Sci. Eng. A* 272 (1999) 114–119, [https://doi.org/10.1016/S0921-5093\(99\)00463-3](https://doi.org/10.1016/S0921-5093(99)00463-3).
- [50] T.Y. Tsui, A.J. McKerrrow, J.J. Vlaskak, The effect of water diffusion on the adhesion of organosilicate glass film stacks, *J. Mech. Phys. Solids* 54 (2006) 887–903, <https://doi.org/10.1016/j.jmps.2005.12.004>.